Discriminative transition sequences of origami metamaterials for mechano-logic

Zuolin Liu, Hongbin Fang, Jian Xu, and K.W. Wang*

Zuolin Liu, Hongbin Fang, Jian Xu
Institute of AI and Robotics, Fudan University, Shanghai, 200092, China
E-mail: fanghongbin@fudan.edu.cn

Zuolin Liu, K.W. Wang
Department of Mechanical Engineering, University of Michigan, Ann Arbor, MI 48109, USA

Keywords: origami, multistability, phase transformation, mechano-logic, physical computing, mechanical metamaterial

Abstract: Transitions of multistability in materials have been exploited for various functions and applications, such as spectral gap tuning, impact energy trapping, and wave steering. However, a fundamental and comprehensive understanding of the transitions, either quasi-static or dynamic transitions, has not yet been acquired, especially in terms of the sequence predictability and tailoring mechanisms. This research, utilizing the stacked Miura-ori-variant (SMOV) structure that has multistable shape reconfigurability as a platform, uncovers the deep knowledge of quasi-static and dynamic transitions, and proposes the corresponding versatile formation and tuning of mechanical logic gates. Through theoretical, numerical, and experimental means, discriminative and deterministic quasi-static transition sequences, including reversible and irreversible ones, are uncovered, where they constitute a transition map that is editable upon adjusting the design parameters. Via applying dynamic excitations and tailoring the excitation conditions, reversible transitions between all stable configurations become attainable, generating a fully-connected transition map. Benefiting from the nonlinearity of the quasi-static and dynamic transitions, basic and compound mechanical logic gates are achieved. The versatility of the scheme is demonstrated by employing a single SMOV to realize different complex logic operations without increasing structural complexity, showing its unique computing power and inspiring the avenue for efficient physical intelligence.

1. Introduction

With the unique merit of exhibiting variable spectral gaps at different stable configurations, multistable mechanical metamaterials have facilitated extensive functions and applications, including phononic bandgap tuning [1,2] and broadband vibration control [3,4]. Among these practices, the multistable metamaterials, which are fundamentally nonlinear in their constitutive profiles, are mainly operating in linear regimes within small deformations around different stable equilibria between configuration transitions. On the other hand, other prospects, such as nonreciprocal wave transmission [5–7], impact energy trapping [8–10], shock isolation [11,12], and transition signal propagation [13–15], have leveraged the nonlinear feature of global multistability, particularly the snap-through transitions among different stable configurations. Recently, there is a growing interest in harnessing multistability for mechanical logic gates [16–18] and mechanical memory devices[19,20] by correlating the mechanical configurations with their digital counterparts. Upon external inputs, the logic operation is determined by the sequence of configuration transitions. While these outcomes are intriguing, the current state-of-the-art technology mainly exploited transitions in an ad-hoc manner, and the underlying mechanics of a transition sequence and the corresponding triggering methods are often not well understood. In other words, systematic and comprehensive investigations into the global transition sequences have not been pursued, which is a major bottleneck that severely limits the robust realization of the many rich functions of multistability.

As a design motif, origami, the ancient art of transforming flat sheets into a sophisticated sculpture through folding, provides potentials in building multistable mechanical metamaterials owing to its large design space and intrinsic geometric nonlinearity [21]. In addition, the scale-independence of the mechanical properties of origami allows it to work at multiple scales, including macroscopic and microscopic scales. The existing precision machining techniques[22] provide us with the possibility to fabricate miniature folding devices. Foreseeable applications include mechanical memory devices[20,23], mechano-logic[18,24,25], and robotics [26–29]. Recently, by incorporating multiple stacked Miura-ori units via a novel stacking strategy[30,31], a new "stacked Miura-ori-variant (SMOV)" structure is created. With unique multistability in inclined and curved directions and multiple configurations, the SMOV becomes a strong candidate for developing smart mechanical metamaterials with directional, configurational, and functional adaptability. Moreover, with 4 to 8 different stable configurations in a single SMOV cell, rich transition sequences are expectable, which brings fresh vitality to the creation of new functions, such as mechano-logic with versatile formation and tuning.

With the abovementioned critical needs in advancing the knowledge of transitions in mechanical multistable metamaterials and the attractive features of SMOV, in this research, our goal is to utilize the SMOV structure as a podium for studying the rich multistability transition behaviors, understanding the underlying physics, and manipulating and harnessing the transition sequences. While this is an exciting opportunity, the complexity of the sequence also brings about major research challenges for us to address, so we can better exploit and leverage the underlying mechanisms of the transitions. Particularly, when transiting the SMOV from one stable configuration to another under rigid-folding, the kinematic bifurcation point[32] (namely, the kinematic singular state) will always be encountered due to the synchronous folding of the constituent cells as a single-degree-of-freedom mechanism. At this point, the SMOV has multiple transition paths via changing the folding direction, which exacerbates the difficulty in elucidating the transition sequence. As a consequence, the subsequent folding of the SMOV becomes indeterminant and unpredictable, which prevents the realization of various SMOV functionalities.

To achieve our research goal, we advance the state of the art by addressing the abovementioned challenges and conducting an investigation of the quasi-static and dynamic transitions among the SMOV multistable configurations. First, we introduce flexibility into the connection between adjacent constituent units, which relaxes the strict rigid-folding kinematic constraints and allows each unit to deform asynchronously, thus making the transition sequence predictable by avoiding the kinematic bifurcation point. In addition, through systematic analysis of the quasi-static configuration switches, transition maps composed of reversible and irreversible transition sequences are revealed. Such transition maps can be further edited by engineering the design parameters of the SMOV structure. Configuration switches can also be triggered by dynamic excitations, in the form of steady-state oscillations around different stable states. Different from the quasi-static scenario, dynamic transitions between any of the two stable equilibria are always reversible, generating a bi-directional full-connected transition map.

Building on this foundation, we discover that the SMOV discriminative transition sequences, including quasi-static and dynamic maps, provide a novel platform for versatile logic operations. Rather than the conventional mechano-logic that a specific structure can only act as a single type of logic gate [16,33,34], the proposed multistable SMOV structure, as a novel element for logic operation, can serve as multiple types of logic gates. Moreover, instead of integrating multiple cells in conventional mechano-logic approaches, our scheme by incorporating a reservoir process can perform compound logic operations based on a single multistable SMOV cell, without increasing structural complexity. These findings, therefore, will inspire the avenue for mechanical intelligence to be harnessed in many systems, e.g., smart materials, MEMS, and robotics.

2. Results

2.1. The Multistable Miura-variant Metamaterial

The Miura-variant metamaterial utilized in this study is constructed by stacking two different Miura-ori sheets, α and β (Figure 1a) as presented in Figure 1b, which includes a large number of tubular cells (Figure 1c). Considering the periodicity, a basic constituent cell of the metamaterial, i.e., a stacked Miura-variant cell, is made up of three units, denoted by A, B, C and are highlighted in Figure 1c their folding motions can be uniquely described by the folding angles $\theta_{A\alpha}$, $\theta_{B\alpha}$, and $\theta_{C\alpha}$. Among them, units A and C are conventional stacked Miura-ori (SMO) units, which possess two different types of configurations, namely, the convex configuration ($\theta_{A\alpha} < 0$ and $\theta_{C\alpha} < 0$) and the concave configuration ($\theta_{A\alpha} > 0$ and $\theta_{C\alpha} > 0$); the newly generated unit, located between units A and C, can also achieve two different types of configurations, the inclined-up ($\theta_{B\alpha} > 0$) and the inclined-down ($\theta_{B\alpha} < 0$) configurations (Figure 1d). Therefore, a single Miura-variant cell can exhibit eight different types of configurations by reconfiguring the constituent units (Figure 1e). In what follows, for clarity, binary codes '1' and '0' are used to represent the convex and concave configuration of units A and C, respectively; 'a' and 'b' are adopted to denote the inclined-down and inclined-up configuration of unit B, respectively. Detailed kinematics of a single cell is presented in Supporting Information, Section S1.

The stability characteristics of a Miura-variant cell are determined by three design parameters: the stiffness ratio, defined as the ratio of the crease torsional spring stiffness per unit length of sheet α (k_α) to that of sheet β (k_β), the stress-free configuration of the cell when there is no internal force, and the corresponding stress-free folding angle (denoted as $\theta^0_{A\alpha}$, $\theta^0_{B\alpha}$, $\theta^0_{C\alpha}$). By tailoring these design parameters, the potential profile of a Miura-variant cell could exhibit different numbers of local minimum, corresponding to different numbers of stable configurations (see detailed derivations of the potential energy in Supporting Information, Section S2). For example, by setting the stress-free configuration at '0-b-0' and allowing the stiffness ratio and the stress-free angle $\theta^0_{A\alpha}$ to vary, the constituent cell could achieve 1, 4, 6, 7, or 8 stable configurations (Figure 1f). For each point on the parameter plane, considering the binary configurations of units B and C, four potential energy curves can be plotted with respect to the folding angle of unit A (i.e., $\theta_{A\alpha}$). For instance, at point P1, all the four curves show prominent double-well characteristics, giving rise to eight stable configurations (Figure 1g top). By reducing the stiffness ratio, the potential wells with relatively shallow depths would disappear, thus reducing the number of stable configurations. Particularly, at point P2, all the four energy curves become mono-stable, producing four stable configurations (Figure 1h top); and at the line with zero stress-free angles (i.e., $\theta^0_{A\alpha} = \theta^0_{B\alpha} = \theta^0_{C\alpha} = 0$), regardless of the stiffness ratio, the four curves completely coincide and share one potential well, which corresponds to the unique stress-free stable configuration. Examples of energy curves with 7, 6, and 1 stable configuration are given in Supporting Information, Figure S2c-e, and evolution of the folding angles at the stable configurations with respect to the stiffness ratio and the stress-free angle is described in Supporting Information, Figure S2a, and Figure S2b, respectively.

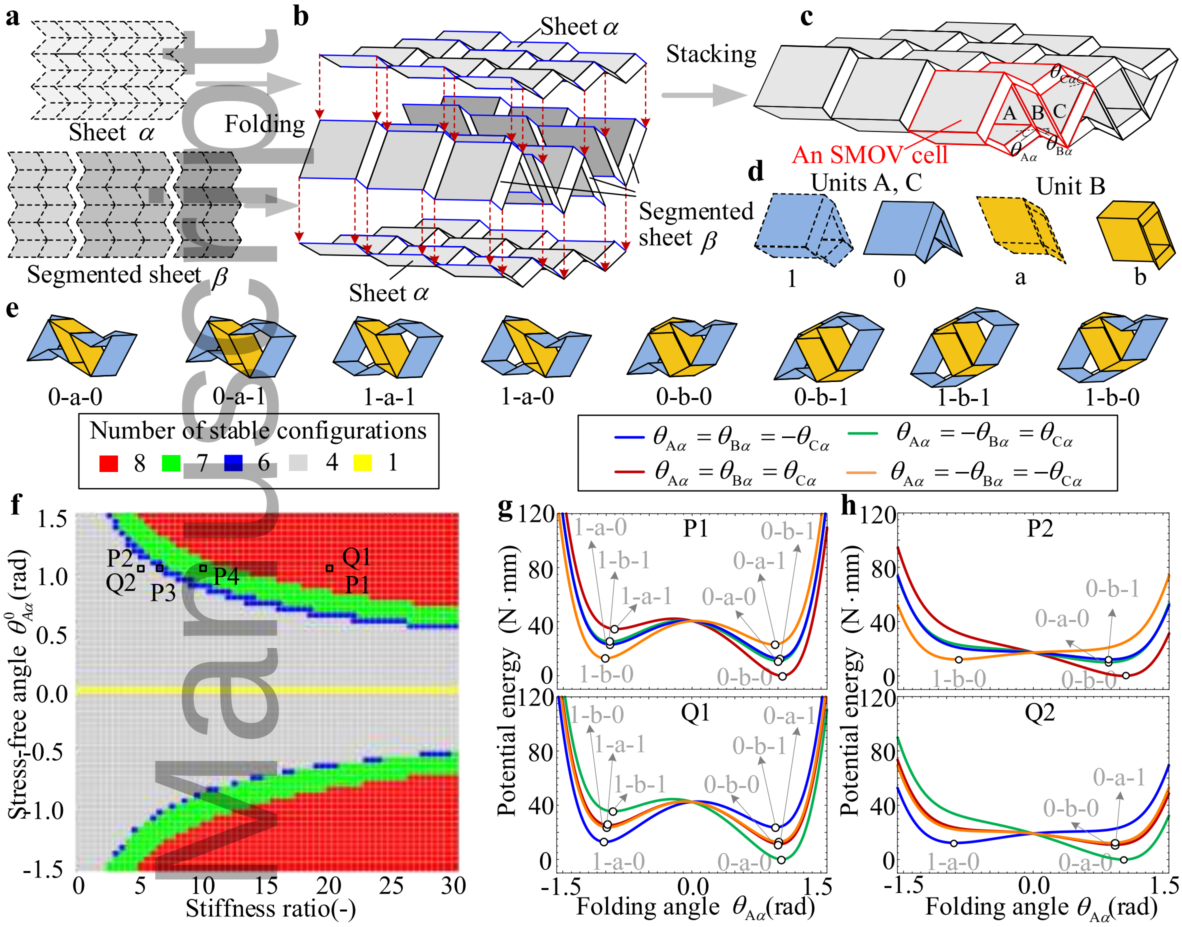

Figure 1. a) Two Miura-ori sheets α and β for constructing the multistable metamaterial. b) Illustration of the stacking method. c) A single layer of the SMOV metamaterial, in which a constituent cell, i.e., a SMOV cell, is highlighted. The SMOV cell is made up of three units, A, B, and C; their kinematics are governed by folding angles $\theta_{A\alpha}$, $\theta_{B\alpha}$, and $\theta_{C\alpha}$, respectively. d) Different configurations of the units. e) Eight different configurations of the SMOV cell. f) Correlation between the number of stable configurations of a SMOV cell and the design parameters (stiffness ratio and stress-free angle). g) and h) Potential energy landscapes of the SMOV cell corresponding to points P1, Q1, P2, and Q2 in f).

Moreover, it is worth noting that even with the same number of stable states, the specific shapes of the stable configurations are still tunable by adjusting the stress-free configuration. For instance, with the same stiffness ratio and stress-free angle but different stress-free configurations (‘0-b-0’ at point P2 and ‘0-a-0’ at point Q2), although the number of stable states remains four, the specific shapes of the stables configuration are not identical, changing from ‘1-b-0’, ‘0-b-1’, ‘0-a-0’, ‘0-b-0’ (Figure 1h, top) to ‘1-a-0’, ‘0-a-1’, ‘0-b-0’, ‘0-a-0’ (Figure 1h, bottom). Similarly, by switching the stress-free configuration from ‘0-b-0’ (point P1) to ‘0-a-0’ (point Q1), the Miura-variant cell remains octa-stable, but the potential energy levels corresponding to the eight stable configurations are changed. Actually, for the Miura-variant cell, the number of stable states can be uniquely determined by the stiffness ratio and the stress-free angles, while the specific shapes of the stable configurations and the related potential energy levels also depend on the stress-free configuration. We will show later that in addition to modifying the overall potential profile of the Miura-variant cell, the three design parameters play a key role in governing the sequences of configuration transitions.

2.2. Quasi-static Transition Sequences

Under the rigid-folding scenario, the kinematic constraints $\theta_{A\alpha} = \pm\theta_{B\alpha} = \pm\theta_{C\alpha}$ have to be precisely satisfied, which forces the three units of the SMOV cell to deform synchronously. Hence, a kinematic bifurcation point with $\theta_{A\alpha} = \theta_{B\alpha} = \theta_{C\alpha}=0$ will always be encountered when transforming the cell among its stable configurations. When passing through this bifurcation point, the sign of the folding angle of each unit cannot be uniquely determined, which makes the transition sequences unpredictable. However, in practice, rigid-foldability cannot be perfectly satisfied due to the inevitable flexibility of the facets and creases, which relaxes the rigid-folding kinematic constraints by allowing each unit to deform asynchronously. Nevertheless, the folding of the adjacent units is not fully independent either; the connecting facets or creases will still impose certain constraints to restrict the folding differences between adjacent units. Specifically, to quantify such imperfect constraints between adjacent units A and B, as well as units B and C in the SMOV cell, two equivalent stiffness k_1^* and k_2^* are introduced; they are applied to the dihedral-angle differences between adjacent units. The quantity of them can be rationally designed by the flexibility of the facets and creases, i.e., more rigid facets and hinge-like creases lead to a larger equivalent stiffness. The newly introduced equivalent stiffness brings about additional potential energy (see detailed derivations in Supporting Information, section S3), which could fundamentally alter the overall potential energy landscape of the SMOV cell. Hence, starting from an initial configuration of the SMOV cell

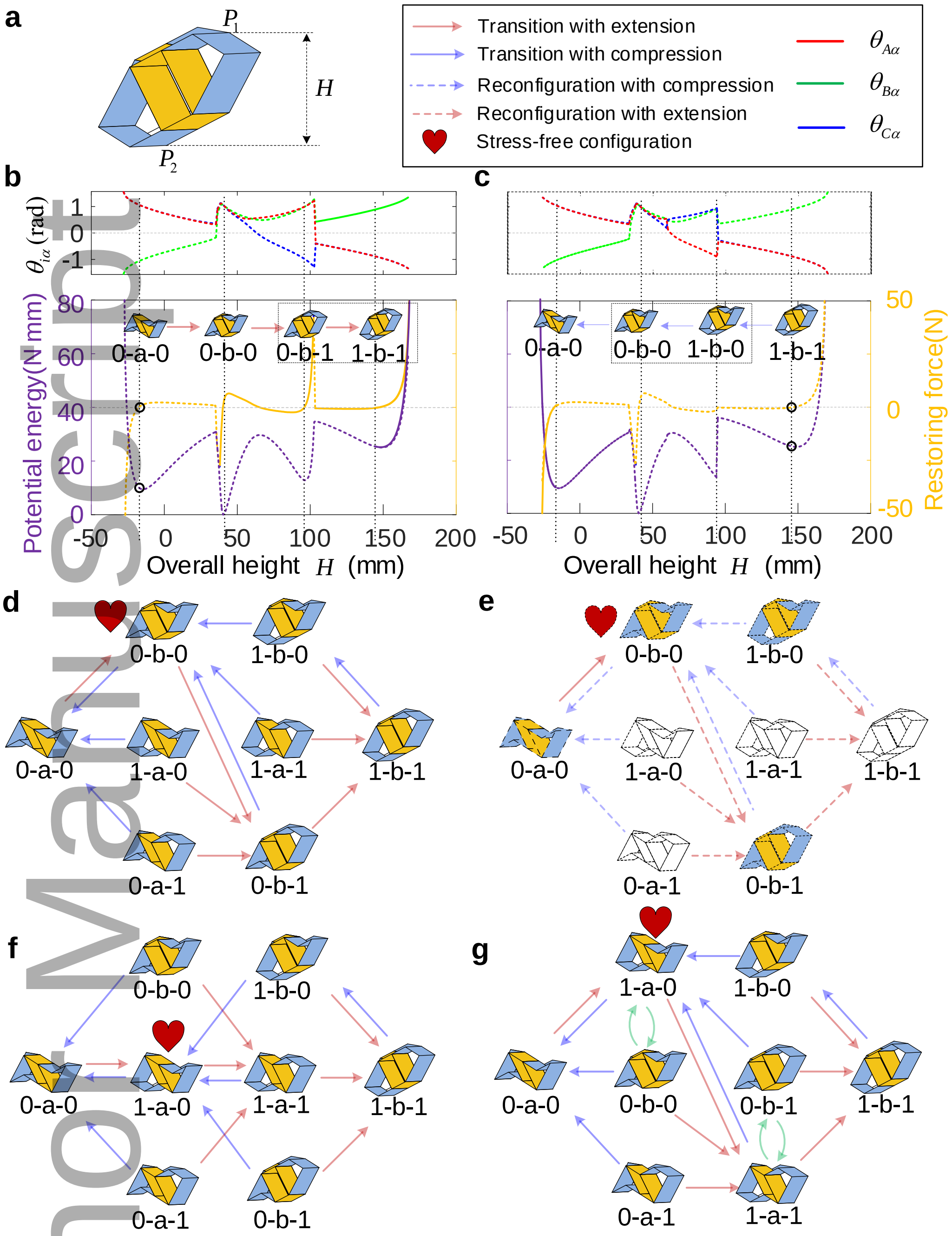

Figure 2. Quasi-static transition sequences of the SMOV cell under the displacement control with design parameters located at P1 in Figure 1f and with equivalent stiffnesses $k_1^* = 500k_\alpha$, $k_2^* = 700k_\alpha$. a) Illustration of the overall height of the SMOV cell. The evolutions of the folding angles of the constituent units A, B, C, the corresponding potential energy, and the restoring force with respect to the overall height with different initial configurations '0-a-0' and '1-b-1' are presented in b) and c), respectively. The black circles and the dotted lines denote the initial configurations and the stable configurations, respectively. The dashed box represents the irreversible transition. The whole transition map obtained by integrating the transition sequences starting from the 8 different initial configurations is shown in d). Configuration marked with heart shape is stress-free. The transition map in e presents the situation with only 4 stable configurations with design parameters located at P2 in Fig 1f (configuration with white color is unstable). f) Transition map with stress-free configurations '1-a-0'. g) is the same map as f but with rearranged positions of the 8 stable configurations. Green arrows denote the configurations which changed their positions in the map.

under displacement control, the path corresponding to the minimum energy can be searched via an optimization process. It is shown that with imperfect constraints, the kinematic bifurcation point is no longer encountered when transiting among the stable configurations, thus making the transition sequence deterministic and predictable. Actually, the transition sequence can be uniquely determined by locating the local minima on the energy landscape.

In the simulation, the equivalent stiffnesses are set as $k_1^* = 500k_\alpha$, $k_1^* = 700k_\alpha$, and the design parameters, i.e., the stiffness ratio, the stress-free angle, and the stress-free configuration, are adopted as $k_\beta = 20k_\alpha$, $\theta_{A\alpha}^0 = \pi/3$, and $\theta_{A\alpha}^0 = \theta_{B\alpha}^0 = \theta_{C\alpha}^0$, respectively ($k_\alpha = 0.01[\mathrm{N/rad}]$). This set of parameters corresponds to point P1 in Figure 1f, where the SMOV cell possesses the largest number of stable configurations (8 stable configurations).

It is worth pointing out that the minimum-energy path search, which is fundamentally an optimization process, closely relates to the loading direction as well as the initial configurations. As a result, to acquire a thorough understanding of the possible transition sequences, displacement controls (including extensions and compressions) starting from different stable configurations are applied to the SMOV cell. For example, with '0-a-0' as the initial configuration and by decreasing the overall height of the SMOV cell (Figure 2a), i.e., compression, the potential energy, and the restoring force will increase sharply (Figure 2b), while the cell will be folded to a flat state ($|\theta_{i\alpha}| \to \pi/2$ $(i = A, B, C)$) without any phase transition. On the contrary, by increasing the height of the SMOV cell from '0-a-0', i.e., extension, three configuration transitions to '0-b-0', '0-b-1', and '1-b-1' are identified via the optimization process, giving rise to a potential energy curve with four wells. Particularly, during the transitions from '0-a-0' to '0-b-0' and '0-b-1' to '1-b-1', the potential energy and the corresponding restoring force experience a discontinuous jump, manifested as a snap-through transition (see the jumps occurred on the folding angles of the constituent units, Figure 2b, top). With the final configuration '1-b-1' as the starting point and by reversing the loading direction, i.e., compressing, a similar four-well potential curve and snap-through transitions are witnessed, while the stable configurations are no longer identical to those in the extension process. The SMOV cell will travel through a new stable configuration '1-b-0', which indicates that the transitions from '0-b-1' to '1-b-1' and from '1-b-0' to '0-b-0' are uni-directional and irreversible. The unidirectional transitions originate from the different deformation paths in the potential energy landscape of the SMOV cell when reversing the loading. With extension or compression, the structure will be deformed toward configurations with larger or smaller overall height. However, for configurations with identical overall height, the structure is always deformed to the one with the lowest potential energy level. Therefore, for the configurations with higher potential energy levels, the deformation path could become irresistible when reversing the loading, giving rise to unidirectional transitions. For example, the transition from '0-b-1' to '1-b-1' is unique with extension since '1-b-1' is the only configuration with a larger overall height than '0-b-1'. However, by reversing the loading direction, i.e., with compression, there are three configurations, '1-b-0', '1-a-1', and '0-b-1', that share the same overall height. Among them, configuration '1-b-0' has the lowest potential energy level and is eventually transformed. Therefore, the transition from '0-b-1' to '1-b-1' becomes unidirectional.

The transition map of the SMOV cell (Figure 2d) can be obtained through the following steps: 1) identify all the eight stable configurations via deriving the minimum potential energy; 2) specify one of the eight stable configurations as the initial state; 3) apply the extension or compression load to the SMOV cell at points P_1 and P_2 along the height direction (H) until the potential energy exceeds a threshold value; 4) record the initial and the experienced states as well as the applied loading direction to get the corresponding transition sequence; 5) repeat the above steps by prescribing each stable configuration as the initial state; 6) integrate all the transition sequences into a complete transition map.

The optimization results corresponding to different initial configurations are presented in Supporting Information, Figure S3. Note that the map is not fully connected, instead, it is made up of uni-directional and bi-directional transitions. By tailoring the design parameters, the reversibility and irreversibility of the transition branches can be changed accordingly, giving rise to qualitatively different transition maps (Supporting Information, Figure S4).

Recall that the stiffness ratio and the stress-free angle play a key role in determining the number of stable configurations. To understand how they affect the transition behavior of the SMOV cell, the transition maps corresponding to point P1 (with eight stable configurations) and point P2 (with four stable configurations) in Figure 1f are illustrated in Figure 2d and 2e, respectively. It reveals that in the transition map corresponding to point P2, configurations '1-a-0', '1-a-1', '1-b-1', and '0-a-1' are unstable (denoted by blank shapes with dashed edges), while the transition paths in the two maps are still identical. This can be interpreted in terms of the potential energy level, which fundamentally determines the transition behaviors. Specifically, although some configurations are no longer stable (Figure 2e), the relative potential energy levels of the SMOV configurations are unchanged (Figure 1h). However, the stress-free configuration, which has been shown to be nonessential to the number of stable configurations, shows its capability to alter the transition sequences of the SMOV cell. For example, by switching the stress-free configuration from '0-b-0' to '1-a-0', the overall transition map is qualitatively changed (Figure 2f): some reversible transitions become irreversible (e.g., between '0-b-0' and '0-a-0'), while some irreversible paths become reversible (e.g., between '0-a-0' and '1-a-0'); moreover, some new transition paths emerge in the new map (e.g., from '1-b-0' to '1-a-0').

Note that configurations '0-b-0' and '1-a-0' correspond to an almost identical height of the SMOV cell, so are configurations '0-b-1' and '1-a-1'. By exchanging the position of '0-b-0' with '1-a-0', and the position of '0-b-1' with '1-a-1' on the map (Figure 2g), the transition paths could remain unchanged as those in Figure 2d. A similar phenomenon is also observed in the case where configuration ‘0-a-1’ serves as the stress-free configuration (Supporting Information, Figure S4c). This can be interpreted from the fact that the transition paths are mainly determined by the overall height and the potential energy level of the SMOV cell. We further examine all the cases with the eight configurations serving as the stress-free states (Supporting Information, Figure S4), and a generic conclusion can be drawn. If the stress-free configurations are of different heights, the relative potential energy relationship among the nodes of the map is changed, and the generated transition maps are fundamentally different; while if the stress-free configurations are of almost identical height (e.g., Supporting Information, Figure S4a~c, and Figure S4d~f), by exchanging the designated configurations with similar height on the map, the relative height and energy relationship among the nodes of the map are retained, thus preserving the transition paths. However, since the designated configurations have been exchanged, the transitions between the two specific configurations are different. Therefore, this generic conclusion on the transition map could also be utilized for tailoring the unidirectional/bidirectional transitions by designating different stress-free configurations.

Note that the optimization process to develop the transition map requires prior knowledge of all the stable configurations. Theoretically, we can determine all the stable configurations of a given multistable metamaterial by deriving the local minima of the potential energy profile. Then extension and compression are respectively applied to each stable configuration to derive the transition sequence in the prescribed loading direction (typically the direction where the structure exhibit evident multistability). The complete transition sequence map is developed by combining all possible sequences. Note that this process may become computationally expensive for an extremely complex multistable mechanical metamaterial. However, some mechanical metamaterials are made up of basic bistable unit cells via periodical connections in series or in parallel, e.g., the multistable metamaterial based on bistable buckled beams[5], Stacked Miura origami[35], and Kresling origami[25]. For these examples, the number of stable configurations can be easily derived, i.e, 2^N, where N is the number of the constituent unit cells. Our SMOV metamaterial falls into this category, which therefore simplifies the analysis.

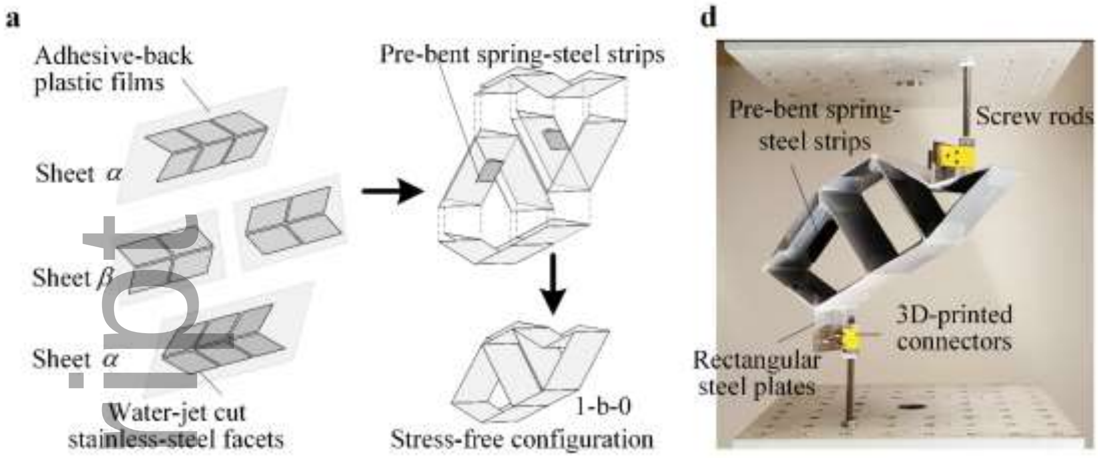

Figure 3 prototype of the origami cell. a) illustration of the prototyping method. d) Experimental setup.

The transition map, consisting of reversible and irreversible transition paths, is also obtained via experiments on a SMOV prototype (Figure 3). The detailed fabrication process is presented in Section 4. With '1-b-0' as the stress-free configuration and '1-b-1' as the initial configuration, by applying compressing displacement control, a series of configuration switches are observed, shown in the time-lapse photo (Figure 4a), and the corresponding force-displacement curve (Figure 4b top, in blue color), also in video S1 in Supporting Information. Note that the points on the curve with zero restoring force correspond to the stable configurations, '1-b-1', '0-b-1', '0-b-0', and '0-a-0', which constitute a chain of transition sequences. With the other stable configurations as the initial states and by applying extension/compression displacement control, different transition sequences can be achieved (Figure 4b and Supporting Information, Videos S2-S6). Integrating these sequences together, the complete transition map can be generated (Figure 4d).

As a comparison, the simulation parameters are adopted as $k_\alpha = 0.0181[\mathrm{N/rad}], k_\beta{=}38.53k_\alpha$, $\theta^0_{A\alpha}{=}-0.6784$, $k_1^* = 214.24k_\alpha$ and $k_2^* = 146.74k_\alpha$, with stress-free configuration '1-b-0' (the identification process to obtain these parameters is presented in S5 in Supporting Information). Accordingly, based on the model with imperfect constraints and the optimization scheme, the transitions can also be obtained via numerical analysis (Figure 4c), which agrees well with the experimental results (Figure 4b) in terms of the number of stable configurations and the overall trend of the force-displacement curves. Quantitatively, the numerical and experimental results are also in good agreement. For example, both numerical simulations and experiments suggest that a small compression force is enough to trigger a snap-through transition from '1-b-1' to '0-b-1'(the blue dashed curve in Figure 4b and 4c, top); while the required extension force for the reverse transition from '0-b-1' to '1-b-1' is much larger (the

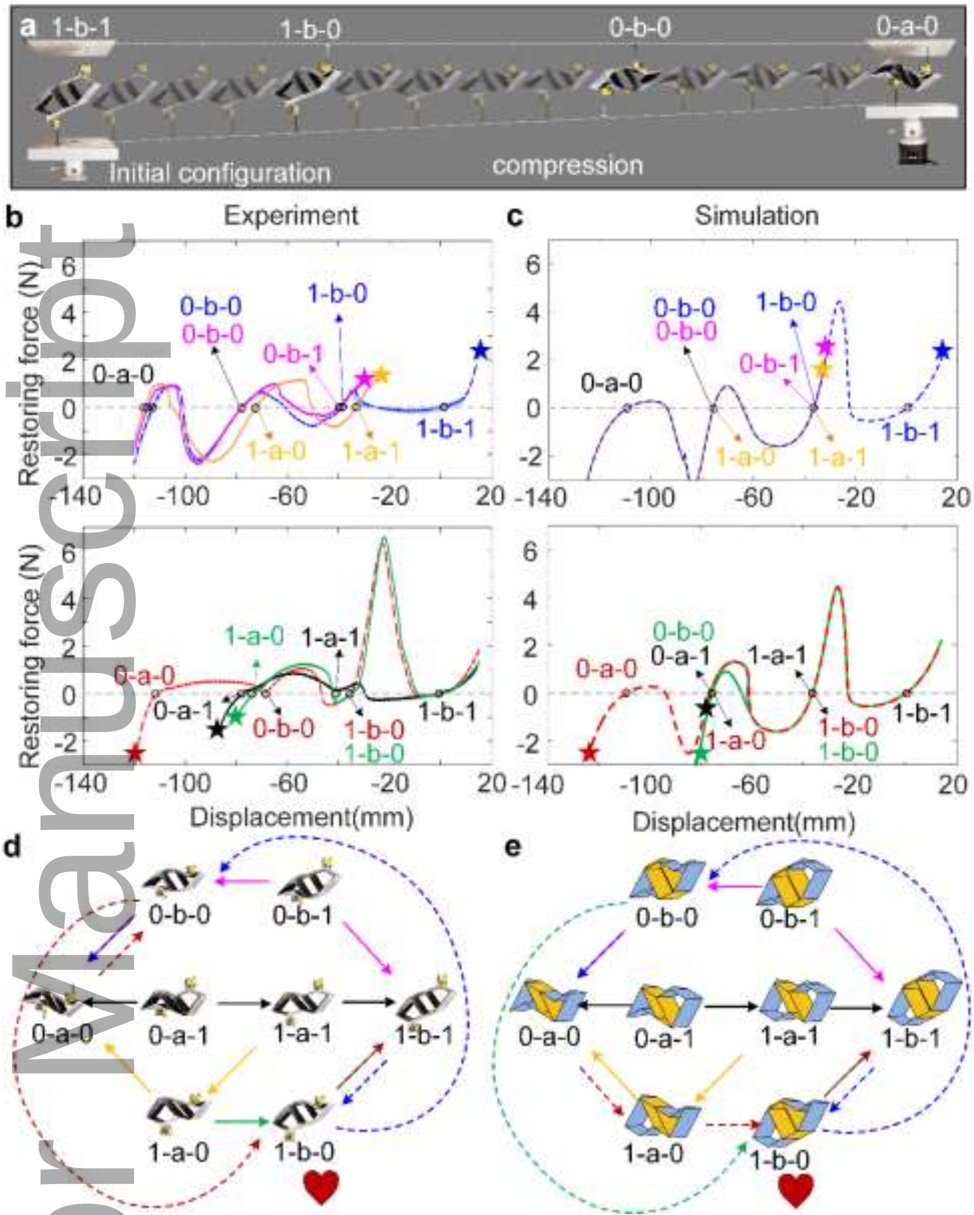

Figure 4. Experimental investigation of the quasi-static transition sequences. a) Time-lapse photo of the SMOV prototype during a quasi-static compression test. b) and c) respectively show the experimental and numerical curves of the restoring force with respect to the external control height. The stars with different colors represent the starting points from different configurations. The corresponding transition paths are denoted by different colored lines. d) and e) are the corresponding transition maps. Configuration marked with heart shape is stress-free. Arrows with different colors denote the transition sequences extracted from different transition paths in b) and c).

red dashed or green curves in Figures 4b and 4c, bottom). Furthermore, comparing the transition maps obtained from experiments (Figure 4d) and simulations (Figure 4e), we see that except for one transition, the two maps, consisting of uni-directional and bi-directional transition paths, exhibit convincing agreement with each other. This again manifests the effectiveness of the modeling and path-searching approaches. Note that the quantitative comparison of the two force-displacement profiles is not so good due to the error of manufacture, identification should be made in order to find accurate parameters.

2.3. Dynamic Transition

In addition to quasi-static control, configuration transitions can be further enriched when the SMOV cell is subject to dynamic excitations. To analyze the dynamics, the kinetic energy of SMOV is examined by summing the kinetic energy of all facets together, where the kinematic energy of a single facet is calculated by area integral. Using the Lagrange equation, the dynamic governing equation of the SMOV cell is derived, shown in Supporting Information, Section S6. When performing the dynamic simulation, the initial state is set at one of the stable configurations with zero velocity, the material density of the facets is set as $\rho = 7.85\,\mathrm{g/cm^3}$, which is the density of steel, the damping coefficient is adopted as $c = 50\mathrm{kg \cdot m/s}$, and the excitation amplitude and frequency are swept. The Runge-Kutta method with variable steps is applied to solve the governing equation. The steady-state response types, in terms of the equilibrium that the system oscillates around, are recorded and shown in a dynamic transition map (Figure 5a), in which the configuration '0-b-1' is set as the initial state. Note that the transitions of the steady-state responses are closely related to the excitations. With relatively small excitation amplitude, the SMOV cell keeps oscillating around the '0-b-1' configuration without change; while with larger excitation amplitudes or higher excitation frequency (i.e., sufficiently high input energy), inter-well oscillations around multiple equilibria will be triggered. In the intermediate region, rich transitions of the steady-state responses are observed, with the surrounded stable equilibrium changing from '0-b-1' to the other seven stable configurations. Similar trends are also witnessed when the other seven stable configurations are set as the initial states (Supporting Information, Figure S8). Being different from the quasi-static scenario in that certain stable configurations cannot be reversibly transformed, here, steady-state oscillations around any of the two stable configurations can be reversibly switched by applying proper dynamic excitations, generating a fully-connected dynamic transition map. Compared with the quasi-static transition, inertial force and damping force are incorporated into the dynamic process. With different inserted energy, the inertial force and damping force will greatly change the transitions among the stable states. By applying excitations with very low frequency, the inertial force, damping force, as well as kinetic energy are very small, which could degenerate the dynamic model into a quasi-static one. In this scenario, the SMOV structure will still follow the quasi-static transition map.

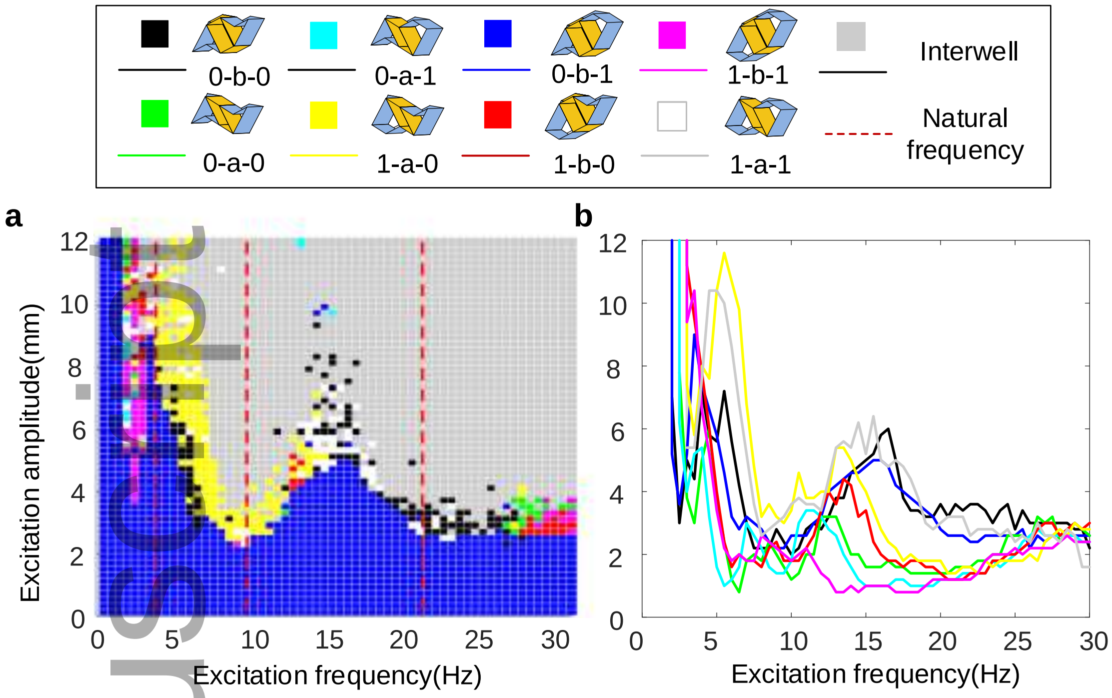

Figure 5. Transition sequences with periodic dynamic control. a) Correlations between the dynamic transitions and the external excitations, i.e., excitation frequency and amplitude. The initial state is at the '0-b-1' configuration with zero initial velocity, and the dashed lines are natural frequencies of the linearized model. b) critical lines triggering transitions with different initial configurations.

The dynamic transition map can be further interpreted from the perspective of resonance. To this end, the dynamic system is linearized around its stable equilibria such that the natural frequencies can be derived (see Supporting Information, Table. S2). In the eight cases shown in Figure 5a and Figure S6, the first three natural frequencies are denoted by red dashed lines. It reveals that around the natural frequencies, the required excitation amplitudes for transitions are obviously lower than those in other frequency ranges. This is because the response amplitude will be amplified significantly due to the resonance effect, which would thus overcome the energy barrier between adjacent stable equilibria and induce a snap-through motion.

To quantify the required energy level for triggering dynamic transitions, the critical curve on each map is extracted, and they are depicted in Figure 5b. Starting from a certain initial state, if the excitation condition locates below the corresponding critical curve, the SMOV cell will keep its intra-well oscillation around the initial stable state. Above the critical curve but below those corresponding to the other initial stable configurations, the stable equilibrium that the steady-state oscillation surrounds are available to change. When the excitation condition locates above all critical curves, large-amplitude inter-well oscillation will take place.

Since the SMOV is highly nonlinear in its constitutive model, the dynamic response is sensitive to the excitations and the initial conditions. Basins of attraction for some stable configurations are presented in Figure S10 of the Supporting Information. It can be concluded that the same transition is always encountered within a certain perturbation range around the initial stable configuration of SMOV under some excitations; while for configuration and excitations with a fractal basin of attraction, it becomes difficult to identify the transitions corresponding to a given initial condition. However, as a potential strategy, the dynamic excitations, if properly harnessed, could greatly enrich the transition sequences.

2.4. Transition Sequences for Mechano-logic

As discussed, under quasi-static loading or dynamic excitations, the SMOV cell could exhibit rich transition behaviors. The transition maps with reversible/irreversible paths are promising in many applications, such as reconfigurable robots and reprogrammable metamaterials. In this research, we especially showcase a novel and unique potential of the SMOV in achieving mechano-logic, the essence of which is the use of mechanical mechanisms as a means of processing information, aiming at endowing computing ability in the mechanical domain.

First of all, the SMOV cell is capable of realizing the functionality of the basic logic gates, i.e., AND, OR, and XOR gates (Figure 6a). Note that digital inputs '0' or '1' are the objects that these logical operation functions will process. Hence, the SMOV cell's stable configurations are encoded. Specifically, for units A and C of the SMOV cell, as the previously used denotation, the 'bulged-out' and the 'nested-in' stable configurations are respectively converted into digits '1' and '0'; for unit B, the 'inclined-up' and the 'inclined-down' stable configurations are respectively put into '1' and '0'. With such encoding, the configurations of the SMOV cell can be represented by three digits (e.g., the initial configuration is assigned to be '0-0-0'). Without loss of generality, the digits of units A and B are specified as the input of the logic gate. The logic operation is achieved by state transitions under a prescribed control, which can be a quasi-static displacement loading or a dynamic excitation. Here, a quasi-static extension process (with only one control step) applied at points P_1 and P_2 along the height direction (the same load condition as in the simulation and experiment) is employed to exemplify the logic operation. Note that for any given stable configuration with extension or compression, the corresponding transition sequence has been experimentally obtained in Figure 4d, i.e., all the transition sequences we used for conducting mechano-logic have been verified in the quasi-static experiment. Therefore, the experiments are no longer repeated in realizing and interpreting the logic gates. By recording the digits of the transited stable configurations in the form of 3-column blocks, an augmented matrix X is constructed (Figure 6a). With one transition, the matrix X consists of two blocks corresponding to the initial and the transformed configurations. In addition to the inputs represented in the first two columns of the matrix X, more columns obtained by state transitions are included. Note that the following blocks corresponding to the next stable configuration rely on the prior stable configuration, the augmented matrix is fundamentally the spatial-temporal pattern of a physical reservoir, which provides rich possibilities for complex logic operation. The output of the logic operation is achieved by a linear readout layer with weights W_{out}, i.e., the output $\hat{Y} = sigmoid(X \cdot W_{out})$. By optimizing the linear weights with *glmfit* function in Matlab, the three logic gates (AND, OR, and XOR) can be successfully realized based on the same SMOV cell (Figure 6a, bottom).

Note that the complete process of the proposed SMOV-based mechano-logic includes encoding, information processing, and readout. In this section, we detailly discuss information processing via the above quasi-static and dynamic transitions of the SMOV, while the encoding and readout processes are simply realized by manual manipulation and by combining the experimental results with the recorded videos, respectively. As a proof of concept, this demonstrates the feasibility of using SMOV for mechano-logic. However, more efforts, such as the integration of actuators and flexible sensors, should be made in the future for more efficient "writing" and "reading".

To understand the importance of state transitions in achieving the logic operations, a direct readout framework without state transitions is illustrated as a comparison (Figure 6b, top). It shows that direct readout from the initial configurations of the SMOV cell could successfully realize the AND and OR gates, however, fail in the XOR operation (Figure 6b, bottom). This is because, for the AND and OR gates, the mapping from the input onto the output is essentially linear, which, as a result, could be distinguished via a direct linear readout classifier. However, the input-output mapping for the XOR gate is nonlinear, and a linear classifier would be inapplicable. On the contrary, by introducing the state transitions (i.e., the physical reservoir, achieved by quasi-static extension) into the operation process (Figure 6a), the initial configurations (i.e., the inputs) can be transited to other stable states, which, fundamentally, is a nonlinear transformation in terms of the digits. As a result, different logic gates, including the ones with nonlinear input-output mapping, can be realized.

More complex logic gates, such as a compound logic shown in Supporting Information, Figure S11a, can also be achieved based on the SMOV cell by adding another input unit and incorporating more control steps (detailed demonstration is presented in Supporting Information, Video S7). Specifically, the fuzzy computing in a compound logic gate, manifesting as connections of multiple AND gates, is equivalently achieved by conducting two transition steps following the transition map and a subsequent linear readout procedure with weights W_{out}. Unlike the conventional mechano-logic approach that multiple basic logic gates

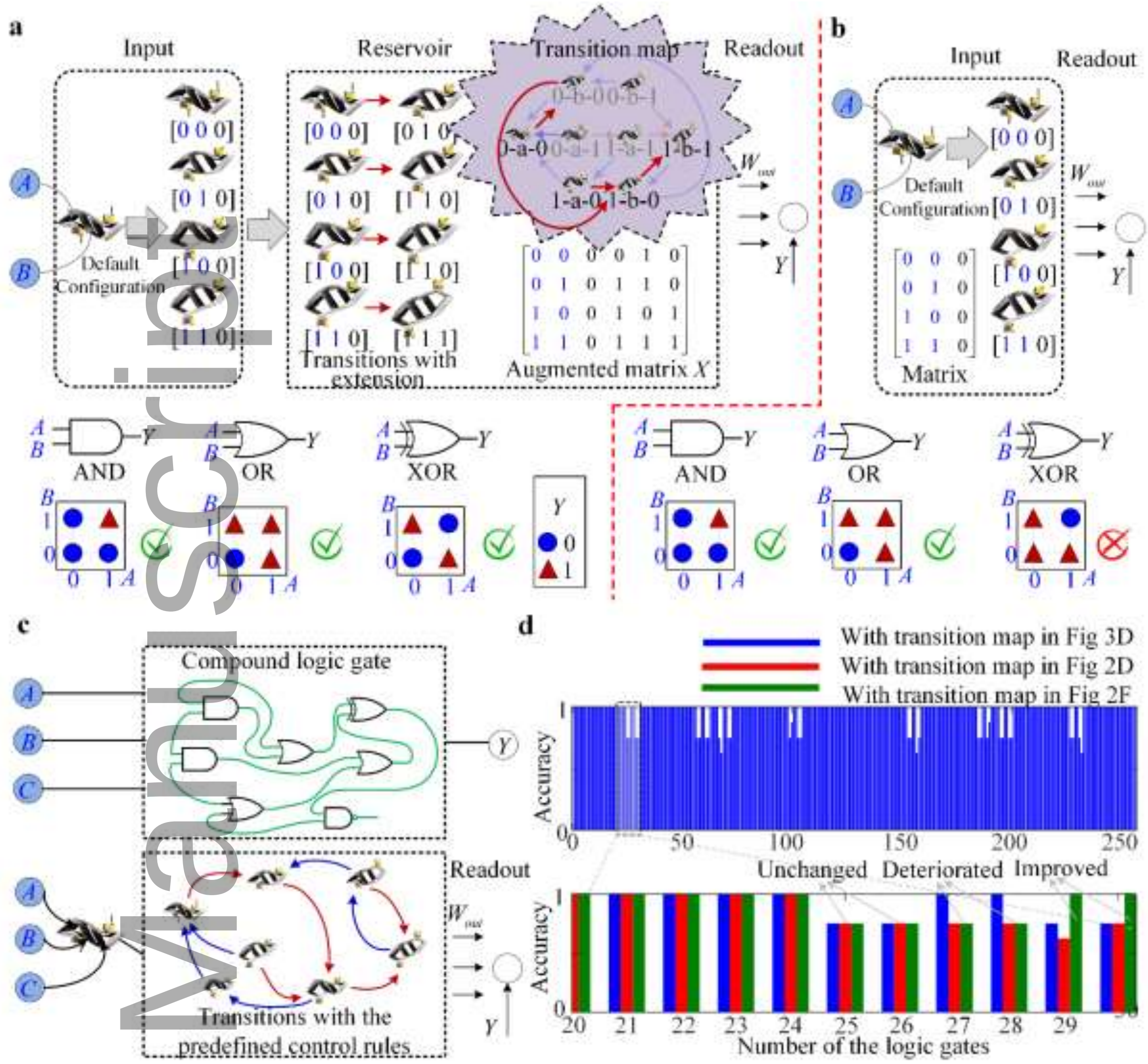

Figure 6. The architecture and results of using the SMOV cell to develop basic logic operations a) with transition procedures, and b) without transition procedures. c) The conceptual framework of developing compound logic gates with three inputs and one output in the electrical scheme and our proposed mechanical scheme. d) Prediction accuracy of using the SMOV cell with different transition maps for all compound logic gates with three inputs and one output. Top: with the experimental transition map; Bottom: comparisons among the three transition maps.

have to be integrated to realize compound logic, our scheme can achieve complex logic operations based on a single SMOV cell, without increasing the structural complexity. This merit originates from the transition behaviors of the multistable SMOV cell, which is a reflection of the nonlinearity of the physical reservoir. As a further example, we demonstrate that a full adder, which is central to most digital circuits that perform addition or subtraction, can also be developed based on a single SMOV cell, see Supporting Information, Figure S11b and Video S8. The three inputs of a full adder are the operands A, B, and the input carry C_{in}; the output of a full adder is the final sum output S and the final carry output C_{out}. With three inputs and two outputs, two transition steps are needed, and an additional set of readout weights (W_{out}^{*}) is incorporated. Note that the versatility of the SMOV cell for different logic operations is closely associated with the readout. The weights of the readout layer are trainable by analyzing the spatial-temporal patterns of the reservoir so that a single SMOV cell is capable of achieving different logic operations. Despite its great flexibility, extra efforts, such as control with additional actuators, are necessary for resetting the SMOV after each logic operation.

Dynamic transitions of the SMOV cell's configurations, which have been shown to be richer than the quasi-static transitions, can also serve as the physical reservoir for logic operations. The difference lies in that a sinusoidal excitation, instead of quasi-static displacement control, is applied to generate the transition sequences (Supporting Information, Figure S11c). With dynamic transition sequences and the associated readout, the SMOV cell can also perform the basic logical operations (i.e., AND, OR, and XOR). For detailed descriptions, see Section S7 in Supporting Information.

Note that for a compound logic gate with three inputs and one output (see a conceptual example in Figure 6c, top), 2^8 different input-output mappings are possible, which correspond to 2^8 logic gates. They can be equivalently achieved via the transitions of the SMOV cell and the trained readout (Figure 6c, bottom). For example, by utilizing the experimental transition map (Figure 4d) and with two transition steps in the proposed scheme, the optimal outputs are obtained with the trained readout weights. Comparing them with the theoretical outputs corresponding to the 2^8 different logic gates, the prediction accuracy is derived. Note that if the accuracy is lower than 100%, the corresponding logic gate cannot be realized. Figure 6d top illustrates the prediction accuracy of the 2^8 logic gates with the experimental transition map. Note that not all the 2^8 logic gates can be accurately achieved. With different transition maps (e.g., the maps shown in Figure 2d and Figure 2f) obtained by adjusting the design parameters of the SMOV cell, the prediction accuracy would be modified. Some of the logic gates that cannot be realized via the experimental transition map are now achievable via another transition map (Figure 6d, bottom). Actually, with different designs of the SMOV cell and different control rules, distinct transition behaviors (i.e., the reservoir) can be obtained, which could be tailored for different mechano-logic. Particularly, if dynamic excitations are used as the control strategy, the fully-connected dynamic transition map could further improve the SMOV logic operations.

3. Conclusion and discussion

A Miura-variant metamaterial with multistable reconfigurable features has been leveraged and investigated as a platform to uncover the deep knowledge and understanding of harnessing multistability transition sequences in both the quasi-static and dynamic realms. By introducing controllable flexibility into the SMOV cell and via a combination of theoretical, numerical, and experimental efforts, rich transition sequences that are predictable and discriminative, including reversible and irreversible paths, are revealed. In addition, the underlying mechanism for editing the transition maps via tailoring the design parameters is uncovered. Dynamic excitations can also trigger transitions, manifested as steady-state oscillations around different stable states. Different from the quasi-static scenario, bi-directional dynamic transitions are accessible between any of the two stable configurations, which constitute a fully-connected transition map. Insights into triggering the transitions are obtained in terms of the resonant frequency and the injected energy.

The SMOV cell, as a representative multistable structure, provides a new path for developing mechano-logic. Based on a single SMOV cell and by harnessing the quasi-static/dynamic transitions as a physical reservoir, basic and complex logical operations are achieved. The proposed framework endows the SMOV cell with the versatility of using one structural element to conduct different logic operations, which greatly reduces the complexity for developing various compound logic gates. Such merit originates from the nonlinearity of the multistable transition. Benefiting from this and by constructing a multi-cell SMOV metamaterial, it is promising in achieving complex computing.

It should be pointed out that anything has a dual character, the SMOV-based mechano-logic is no exception. Compared with the conventional mechano-logic, the structural complexity is greatly reduced, however, at the cost of introducing additional actuation and sensing devices for encoding and resetting. With dynamic excitations, theoretically speaking, one actuator could realize all the encoding and computing processes, however, this requires more effort on an accurate and robust control. Currently, we only demonstrate the computing capability of SMOV with quasi-static and dynamic transitions. In the future, we expect that flexible sensors and active materials could be embedded in the SMOV metamaterial, such that the metamaterial could be more intelligent with integrated sensing, computing, and actuation.

4. Experimental Section/Methods

The fabrication process of the prototype is explained as follows: the facets are water jet cut individually from 0.25-mm-thick stainless steel sheets. Then they are connected to a 0.13-mm-thick adhesive-back plastic film [ultrahigh molecular weight (UHMW) polyethylene] to form the prescribed two different Miura-ori sheets, see Figure 3a. After that, we fold the sheets in the way presented in Figure 3a and paste 0.01-mm-thick pre-bent spring-steel stripes at the corresponding creases to provide torsional stiffness. In this way, the stiffness ratio is greatly increased, which will generate more stable configurations. The stress-free angle corresponding to a stress-free configuration is about $-\pi/3$. Then the sheets are connected along the connecting creases by adhesive films to form a complete single-cell prototype. Therefore, the stress-free configuration is '1-b-0'. In the experiment, we design a 3D-printed connector, which can be screwed onto the prototype with rectangular steel plates. A screw rod is then utilized to connect the 3D-printed connector with the Instron machine (Figure 3b).

Supporting Information

Supporting Information is available from the Wiley Online Library or from the author.

Acknowledgements

Z.L., H.F., and J.X. acknowledge the supports from the National Key Research and Development Project of China under Grant No. 2020YFB1312900 and the Key Project of the National Natural Science Foundation of China under Grant No. 11932015. Z.L. also acknowledges the China Postdoctoral Science Foundation under Grant No. 2021TQ0071 and 2021M700819, and H.F. acknowledges the National Natural Science Foundation of China under Grant No. 11902078. This research is also partially supported by the University of Michigan Collegiate Professorship.

Received: ((will be filled in by the editorial staff))

Revised: ((will be filled in by the editorial staff))

Published online: ((will be filled in by the editorial staff))

References

[1] S. Babaee, N. Viard, P. Wang, N. X. Fang, K. Bertoldi, *Adv. Mater.* **2016**, *28*, 1631.

[2] O. R. Bilal, A. Foehr, C. Daraio, *Proc. Natl. Acad. Sci. U. S. A.* **2017**, *114*, 4603.

[3] Z. Ren, L. Ji, R. Tao, M. Chen, Z. Wan, Z. Zhao, D. Fang, *Extrem. Mech. Lett.* **2021**, *42*, 101077.

[4] J. Meaud, K. Che, *Int. J. Solids Struct.* **2017**, *122–123*, 69.

[5] G. Librandi, E. Tubaldi, K. Bertoldi, *Nat. Commun.* **2021**, *12*, 3454.

[6] Y. Zheng, Z. Wu, X. Zhang, K. W. Wang, *Smart Mater. Struct.* **2019**, *28*, 045005.

[7] Z. Wu, K. W. Wang, *J. Sound Vib.* **2019**, *458*, 389.

[8] S. Shan, S. H. Kang, J. R. Raney, P. Wang, L. Fang, F. Candido, J. A. Lewis, K. Bertoldi, *Adv. Mater.* **2015**, *27*, 4296.

[9] X. Tan, B. Wang, K. Yao, S. Zhu, S. Chen, P. Xu, L. Wang, Y. Sun, *Int. J. Mech. Sci.* **2019**, *164*, 105168.

[10] S. Jeon, B. Shen, N. A. Traugutt, Z. Zhu, L. Fang, C. M. Yakacki, T. D. Nguyen, S. H. Kang, *Adv. Mater.* **2022**, *34*, 2200272.

[11] T. Frenzel, C. Findeisen, M. Kadic, P. Gumbsch, M. Wegener, *Adv. Mater.* **2016**, *28*, 5865.

[12] H. Yang, L. Ma, *J. Mater. Sci.* **2019**, *54*, 3509.

[13] H. Yasuda, L. M. Korpas, J. R. Raney, *Phys. Rev. Appl.* **2020**, *13*, 054067.

[14] L. Jin, R. Khajehtourian, J. Mueller, A. Rafsanjani, V. Tournat, K. Bertoldi, D. M. Kochmann, *Proc. Natl. Acad. Sci. U. S. A.* **2020**, *117*, 2319.

[15] N. Nadkarni, A. F. Arrieta, C. Chong, D. M. Kochmann, C. Daraio, *Phys. Rev. Lett.* **2016**, *116*, 244501.

[16] Y. Song, R. M. Panas, S. Chizari, L. A. Shaw, J. A. Jackson, J. B. Hopkins, A. J. Pascall, *Nat. Commun.* **2019**, *10*, 882.

[17] Y. Jiang, L. M. Korpas, J. R. Raney, *Nat. Commun.* **2019**, *10*, 128.

[18] H. Yasuda, P. R. Buskohl, A. Gillman, T. D. Murphey, S. Stepney, R. A. Vaia, J. R. Raney, *Nature* **2021**, *598*, 39.

[19] T. Chen, M. Pauly, P. M. Reis, *Nature* **2021**, *589*, 386.

[20] H. Yasuda, T. Tachi, M. Lee, J. Yang, *Nat. Commun.* **2017**, *8*, 962.

[21] S. Li, H. Fang, S. Sadeghi, P. Bhovad, K. Wang, *Adv. Mater.* **2019**, *31*, 1805282.

[22] S. Chen, J. Chen, X. Zhang, Z.-Y. Li, J. Li, *Light Sci. Appl.* **2020**, *9*, 75.

[23] T. Jules, A. Reid, K. E. Daniels, M. Mungan, F. Lechenault, *Phys. Rev. Res.* **2022**, *4*, 013128.

[24] B. Treml, A. Gillman, P. Buskohl, R. Vaia, *Proc. Natl. Acad. Sci. U. S. A.* **2018**, *115*, 6916.

[25] L. S. Novelino, Q. Ze, S. Wu, G. H. Paulino, R. Zhao, *Proc. Natl. Acad. Sci. U. S. A.* **2020**, *117*, 24096.

[26] J. Kaufmann, P. Bhovad, S. Li, *Soft Robot.* **2021**, *00*, soro. 2020.0075.

[27] S. Wu, Q. Ze, J. Dai, N. Udipi, G. H. Paulino, R. Zhao, *Proc. Natl. Acad. Sci. U. S. A.* **2021**, *118*, e2110023118.

[28] Q. Ze, S. Wu, J. Nishikawa, J. Dai, Y. Sun, S. Leanza, C. Zemelka, L. S. Novelino, G. H. Paulino, R. Renee Zhao, *Sci. Adv* **2022**, *8*, eabm7834.

[29] A. Pagano, T. Yan, B. Chien, A. Wissa, S. Tawfick, *Smart Mater. Struct.* **2017**, *26*, 094007.

[30] Z. Liu, H. Fang, J. Xu, K. W. Wang, *Smart Mater. Struct.* **2021**, *30*, 085029.

[31] Z. Liu, H. Fang, J. Xu, K. W. Wang, In *Volume 10: 44th Mechanisms and Robotics Conference (MR)*, American Society of Mechanical Engineers, **2020**, p. V010T10A082.

[32] Y. Chen, J. Yan, J. Feng, *Symmetry (Basel).* **2019**, *11*, 1101.

[33] Z. Meng, W. Chen, T. Mei, Y. Lai, Y. Li, C. Q. Chen, *Extrem. Mech. Lett.* **2021**, *43*, 101180.

[34] C. El Helou, P. R. Buskohl, C. E. Tabor, R. L. Harne, *Nat. Commun.* **2021**, *12*, 1633.

[35] S. Sengupta, S. Li, *J. Intell. Mater. Syst. Struct.* **2018**, *29*, 2933.

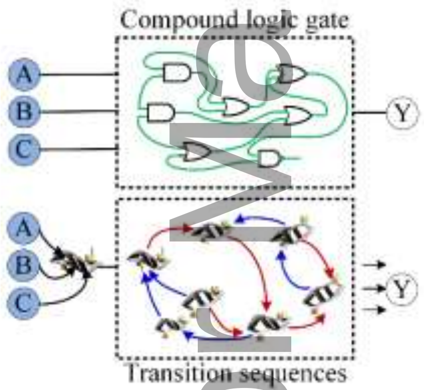

With innovation that reveals the predictability and discriminability of the quasi-static and dynamic transition sequences, new knowledge of the transition mechanics is created. Moreover, the unique mechanical computing strength of the transition sequences for conducting logic operations is uncovered. Basic and various compound logic gates are achievable with a single stacked Miura-ori-variant structure.